Large phonon band gap in $SrTiO_3$ and the vibrational signatures of ferroelectricity in $ATiO_3$ perovskites: First-principles lattice dynamics and inelastic neutron scattering

Narayani Choudhury,[1] Eric J. Walter,[2] Alexander I. Kolesnikov,[3] and Chun-Keung Loong[3]
[1]*Solid State Physics Division, Bhabha Atomic Research Centre, Trombay, Mumbai 400085, India*
[2]*Department of Physics, College of William and Mary, Williamsburg, Virginia 23187, USA*
[3]*Intense Pulsed Neutron Source Division, Argonne National Laboratory, Argonne, Illinois 60439, USA*
(Received 5 February 2008; revised manuscript received 12 March 2008; published 23 April 2008)

We report on first-principles density functional perturbation theory calculations and inelastic neutron scattering measurements of the phonon density of states, dispersion relations, and electromechanical response of $PbTiO_3$, $BaTiO_3$, and $SrTiO_3$. The phonon density of states of the quantum paraelectric $SrTiO_3$ is found to be fundamentally distinct from that of ferroelectric $PbTiO_3$ and $BaTiO_3$ with a large, 70–90 meV, phonon band gap. The phonon dispersion and electromechanical response of $PbTiO_3$ reveal giant anisotropies. The interplay of covalent bonding and ferroelectricity strongly modulates the electromechanical response and gives rise to spectacular signatures in the phonon spectra. The computed charge densities have been used to study the bonding in these perovskites. Distinct bonding characteristics in the ferroelectric and paraelectric phases give rise to spectacular vibrational signatures. While a large phonon band gap in $ATiO_3$ perovskites seems to be a characteristic of quantum paraelectrics, anisotropy of the phonon spectra correlates well with ferroelectric strength. These correlations between the phonon spectra and ferroelectricity can guide future efforts at custom designing still more effective piezoelectrics for applications. These results suggest that vibrational spectroscopy can help design novel materials.

DOI: 10.1103/PhysRevB.77.134111 PACS number(s): 63.20.D−, 71.15.Mb, 77.80.−e, 78.70.Nx

I. INTRODUCTION

Ferroelectric materials interconvert electrical and mechanical energies and find key technological applications[1] as piezoelectric transducers and actuators used in ultrasonic devices, medical imaging, and telecommunications. Classic perovskites such as $PbTiO_3$, $BaTiO_3$, and $SrTiO_3$ present unusual properties and puzzles[1–23] and their first-principles calculations[2–12] and experiments[13–23] have helped elucidate a wide range of fundamental issues such as the electronic origins of ferroelectricity,[3] soft phonon modes and structural phase transitions,[1,13] giant longitudinal optic (LO)–transverse optic (TO) splittings[7] and vibrational anomalies,[4–9] origin of ultrahigh electromechanical response,[10] etc. $SrTiO_3$ is an incipient ferroelectric with a very large static dielectric response, which exhibits remarkable phonon anomalies[5,18] and electrostrictive response.[19] The ferroelectric phase in $SrTiO_3$ is suppressed even as $T \rightarrow 0$ K by zero-point fluctuations, leading to quantum paraelectricity.[15]

Both $PbTiO_3$ and $BaTiO_3$ have a simple cubic high temperature paraelectric phase, which transforms to a ferroelectric tetragonal phase around 763 and 403 K, respectively.[1] Tetragonal $PbTiO_3$ is a large strain material ($c/a=1.06$), which is ferroelectric even at high temperatures and exhibits a single cubic to tetragonal transition. $BaTiO_3$, on the other hand, has a much smaller strain (1.01) and exhibits successive phase transitions from cubic to tetragonal, orthorhombic, and rhombohedral structures with decreasing temperature. $SrTiO_3$ undergoes a transition from the cubic ($Pm\bar{3}m$) to a tetragonal ($I4/mcm$) antiferrodistortive phase at 105 K; however, this transition has a nonpolar character and does not affect its dielectric properties. Electronic structure calculations[3] reveal that intrinsic differences in the bonding in tetragonal $BaTiO_3$ and $PbTiO_3$ give rise to their vastly different phase diagrams and ferroelectric behaviors.

In this work, we report on *ab initio* lattice dynamics calculations and inelastic neutron scattering studies of the complete phonon dispersion relations, density of states, and electromechanical response of three classic perovskites: ferroelectric $PbTiO_3$ and $BaTiO_3$ and the quantum paraelectric $SrTiO_3$. The experimental and theoretical determination of the phonon density of states and dispersion relations gives access to valuable quantitative information concerning elasticity, piezoelectric and dielectric behaviors, thermodynamic properties, and the dynamics of soft-mode driven phase instabilities. While the phonon dispersion relations determine various electromechanical tensor properties, the phonon density of states is the key quantity that governs the thermodynamic properties. The fundamental interest, distinct ferroelectric behavior, and important applications make $PbTiO_3$, $BaTiO_3$, and $SrTiO_3$ highly suitable for these studies. Our goals are (i) to understand the vibrational signatures of ferroelectricity, (ii) to study the interplay between the structure, bonding, dynamics, and electromechanical response, and (iii) to identify the factors that govern the enhanced piezoelectric response, which is required for the design of new materials. The neutron measurements provide a critical test for the theory. The integration of first-principles calculations and vibrational spectroscopic experiments provide important insights into the correlations between vibrational spectra and ferroelectricity and illustrate how vibrational spectroscopic techniques can lead to the design of novel materials.

Several workers[20] have reported inelastic neutron scattering measurements of the phonon dispersion relations and have studied the temperature variations in the soft phonon mode across the ferroelectric to paraelectric transition in these perovskites. The phonon dispersion relation data are,

however, incomplete especially in the lower symmetry ferroelectric phases. Even in the high symmetry paraelectric cubic phase, the dispersion relations of only the acoustic and low frequency optic phonon branches have been measured.[20] Thus far, first-principles calculations of the complete phonon dispersion relations are reported only for the cubic phases[2,6] of $PbTiO_3$, $BaTiO_3$, and $SrTiO_3$. A thorough understanding of the phonon dispersion relations in the ferroelectric phases is essential for a microscopic understanding of their electromechanical properties and for resolving the controversies about the origin of diffuse scattering[23] in perovskite ferroelectrics and have formed the focus of this work. In spite of a flurry of reported research on these perovskites,[1–23] studies of the complete phonon density of states and systematic examinations of the vibrational signatures of ferroelectricity, etc., were not studied earlier. A systematic examination of these various issues, which form the fundamental link between the microscopic physics and macroscopic material behavior, is the key to defining new experimental protocols for the screening and design of novel functional materials. Classic perovskites such as $PbTiO_3$, $BaTiO_3$, and $SrTiO_3$, which have served as a fertile ground for the discovery of new physical phenomena and devices,[1–23] are ideal model systems for such studies.

II. TECHNIQUES

A. Theoretical studies

We have undertaken first-principles calculations of ferroelectric tetragonal $PbTiO_3$ and rhombohedral $BaTiO_3$ with space groups $P4mm$ and $R3m$ and the paraelectric cubic ($Pm\bar{3}m$) and antiferrodistortive tetragonal phases ($I4/mcm$) of $SrTiO_3$ (ST). Density functional theory (DFT) permits calculation of the total energy of solids without any parametrization to experimental data. The phonon spectra and elastic, piezoelectric, and dielectric tensors are related to the second derivates of the total energy with respect to variables such as atomic displacements, macroscopic strain, and electric field. All these material properties can be efficiently computed using density functional perturbation theory (DFPT).[24–27] The dielectric susceptibility and elastic constants involve second derivatives of the total energy with respect to electric field and strain, respectively, while the piezoelectric tensor is the mixed second derivative of the total energy with respect to strain and electric field. DFPT linear response studies have intrinsic advantages over the frozen phonon technique, because they do not require large supercells for the studies of phonons at a general wave vector. Furthermore, the DFPT approach includes explicit treatment of the long-ranged Coulomb interactions, which are required to obtain accurate values of the LO-TO splittings.

We carried out DFT and DFPT linear response calculations by using plane-wave basis sets and the code ABINIT (Ref. 28) by using the local density approximation (LDA). These calculations used norm-conserving pseudopotentials[29,30] generated using the code OPIUM. The pseudopotential results were rigorously tested[31] against the full-potential linearized augmented plane-wave calculations and included appropriate semicore states as valence states. The Brillouin zone integrations were performed with a $6\times6\times6$ **k**-point mesh by using a plane-wave energy cutoff of 120 Ry. We first carried out full structural relaxations for these perovskites. Linear response DFPT studies[24–26,31,32] using a $6\times6\times6$ **k**-point grid with atomic displacements, strain, and electric field perturbations were used to compute the zone center phonon frequencies and elastic, piezoelectric, and dielectric properties. The spontaneous polarization was computed using Berry's phase approach[27] by using a $6\times6\times20$ **k**-point grid, with a dense mesh along the direction of polarization. All calculations are at zero temperature.

To study the phonons at a general wave vector, response functions were calculated on a $4\times4\times4$ grid of **q** points in the Brillouin zone (BZ), including the zone center Γ point. The phonon frequencies at a general wave vector **q** were obtained by interpolating the dynamical matrices calculated on this grid. The phonon density of states involves an integrated average over the phonon modes in the entire Brillouin zone and is given by

$$g(\omega) = A \int_{BZ} \sum_{j} \delta[\omega - \omega_j(\mathbf{q})] d\mathbf{q},$$

where A is a normalization constant such that $\int g(\omega) d\omega = 1$ and $\omega_j(\mathbf{q})$ is the frequency of the j^{th} phonon mode having energy $E_j(\mathbf{q}) = \hbar\omega_j(\mathbf{q})$. We used a $12\times12\times12$ **q**-point mesh in the irreducible Brillouin zone to calculate the phonon density of states.

B. Experimental studies

We have carried out inelastic neutron scattering measurements ($T=6$ K) of the phonon density of states of three classic perovskites: ferroelectric $PbTiO_3$ and $BaTiO_3$ and the quantum paraelectric $SrTiO_3$. The inelastic neutron scattering measurements were carried out using powder samples on the High-Resolution Medium-Energy Chopper Spectrometer (HRMECS) by using the time-of-flight technique at Argonne's Intense Pulsed Neutron Source. Two incident-neutron energies were used (50 and 130 meV) to obtain good resolution data in all ranges of energy transfers. The data were collected over a wide range of scattering angles (28°–132°) for a large coverage of momentum transfers. The high energies of neutrons from pulsed sources enable measurements of the phonon spectra over its entire energy range. Samples were cooled to 6 K using a conventional liquid-helium cryostat with the sample to minimize multiphonon contributions. The energy resolution ΔE (full width at half maximum) of the HRMECS spectrometer varies between 2% and 6% of the incident-neutron energy (E_0) over the neutron-energy-loss region. The data were corrected for background scattering by subtracting the results from empty container runs. Measurements of the elastic incoherent scattering from a vanadium standard provided the detector calibration and intensity renormalization.

The observed data were analyzed in the incoherent approximation,[33,34] wherein the measured scattering function $S(Q,E)$ in the neutron-energy-loss experiments is related to the generalized density of states by[34]

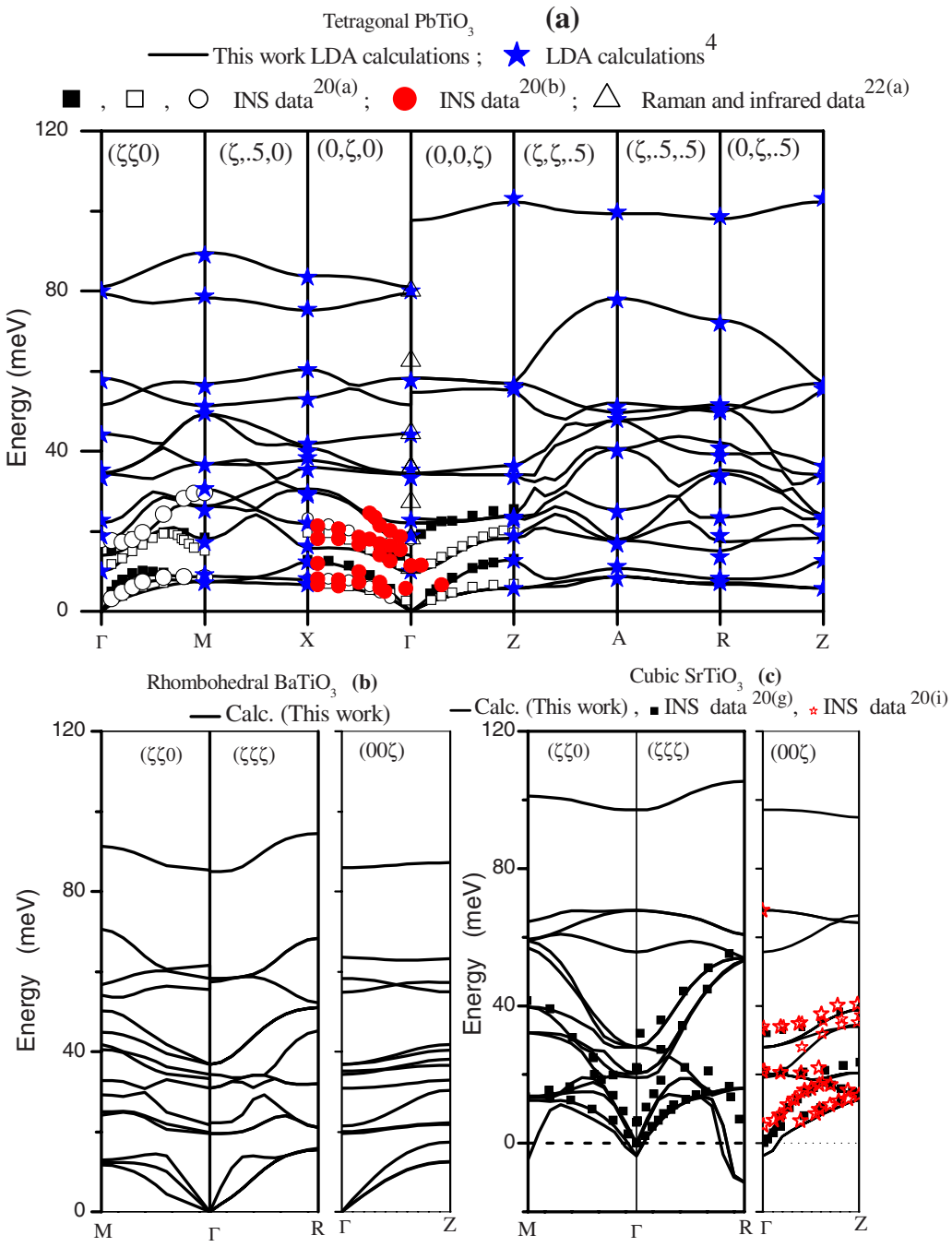

FIG. 1. (Color online) Computed phonon dispersion relations (full line) of (a) tetragonal $PbTiO_3$, (b) rhombohedral $BaTiO_3$, and (c) cubic $SrTiO_3$ compared to reported experimental inelastic neutron scattering (INS) single crystal data (Ref. 20), optical long-wavelength data [Ref. 22(a)], and reported first-principles calculations (Ref. 4).

$$g^n(E) = B\left\langle \frac{e^{2W(Q)}}{Q^2}\frac{E}{n(E,T)+1}S(Q,E)\right\rangle \approx C\sum_k \left\{\frac{4\pi b_k^2}{m_k}\right\} g_k(E),$$

where the partial density of states $g_k(E)$ is given by

$$g_k(E) = D\int_{BZ}\sum_j |\xi(\boldsymbol{qj},k)|^2 \delta(E - E_j(\boldsymbol{q}))d\boldsymbol{q}$$

and

$$n(E,T) = [\exp(E/k_BT) - 1]^{-1}.$$

B, C, and D are normalization constants. b_k and m_k are, respectively, the neutron scattering length and mass of the kth atom. $E_j(\boldsymbol{q})$ and $\xi(\boldsymbol{qj})$ correspond, respectively, to the energy and eigenvector of the jth phonon mode at wave vector $\mathbf{q}$ in the BZ. The symbol $\langle\,\rangle$ represents Q averaging of the quantities within.

TABLE I. Calculated structural parameters and long-wavelength phonon frequencies ω (cm^{-1}) of tetragonal $PbTiO_3$ and rhombohedral $BaTiO_3$ compared to reported experimental [Refs. 1(b), 21, and 22(a)] x-ray and neutron diffraction, Raman, and infrared data. For tetragonal $PbTiO_3$, the z atomic coordinates are given in lattice units. The $R3c$ structure of $BaTiO_3$ is defined by the lattice constant a (Å), rhombohedral angle (in degree), and atomic displacements relative to ideal cubic positions Δ (Å). The calculated polyhedral (PbO_8, BaO_{12}) and TiO_6 octahedral distortions and bond lengths of $PbTiO_3$ and $BaTiO_3$ are in good agreement with the experimental data. The numbers in parentheses after the bond-lengths give the multiplicity of the bonds. Symmetry analysis of the zone-center Γ-point phonon modes for the $P4mm$ space group of $PbTiO_3$ yields the classification $\Gamma: 4A_1+5E+B_1$. The E-symmetry phonon modes are doubly degenerate. For rhombohedral $BaTiO_3$, the phonon modes can be classified as $\Gamma: 4A_1+5E+A_2$. The LO and TO phonon frequencies of the polar modes are listed.

		LDA calculations (this work)	LDA calculations [Refs. 4 and 26(b)]	Experiment [Refs. 1(b), 21, and 22(a)]
$PbTiO_3$	a (Å)	3.9048	3.9048[a]	3.9048,[b] 3.902[c]
	c/a	1.063	1.063[a]	1.063,[b] 1.065[c]
	z(Ti)	0.5378	0.549[a]	0.54,[b] 0.5377[c]
	z(O1,O2)	0.6145	0.630[a]	0.612,[b]0.6118[c]
	z(O3)	0.1136	0.125[a]	0.112,[b] 0.1117[c]
	Pb-O (Å)	2.8016(4), 2.5243(4)		2.7980(4),[c] 2.5319(4)[c]
	Ti-O (Å)	1.9785(4), 1.7606(1), 2.3908(1)		1.9751(4),[c] 1.7700(1),[c] 2.3860(1)[c]
	A_1 (TO) (cm^{-1})	146, 355, 648	151,[a] 355,[a] 645,[a]	147,[d] 359,[d] 646[d]
	A_1 (LO) (cm^{-1})	187, 438, 781	187,[a] 449,[a] 886,[a]	189,[d] 465,[d] 796[d]
	E (TO) (cm^{-1})	90, 170, 275, 465	81,[a] 183,[a] 268,[a] 464,[a]	88,[d] 220,[d] 289,[d] 505[d]
	E (LO) (cm^{-1})	117, 275, 416, 635	114,[a] 267,[a] 435,[a] 625[a]	128,[d] 289,[d] 436,[d] 723[d]
	B_1 (cm^{-1})	277	285[a]	289[d]
$BaTiO_3$	a (Å)	4.0	4.0[e]	4.0[f]
	θ (deg)	89.90	89.85[e]	89.90[f]
	Δ_z(Ti) (Å)	0.053	0.043[e]	0.052 ± 12[f]
	Δ_x(O) (Å)	−0.052	−0.049[e]	-0.044 ± 8[f]
	Δ_z(O) (Å)	−0.080	−0.077[e]	-0.072 ± 8[f]
	Ba-O (Å)	2.8286(6), 2.7335(3), 2.911(3)		2.8287(6),[g] 2.7739(3),[g] 2.8981(3)[g]
	Ti-O (Å)	1.864(3), 2.147(3)		1.8776(3),[g] 2.1351(3)[g]
	A_1 (TO) (cm^{-1})	167, 295, 527	169,[e] 255,[e] 511[e]	
	A_1 (LO) (cm^{-1})	183, 462, 679	179,[e] 460,[e] 677[e]	
	E (TO) (cm^{-1})	162, 240, 468, 296[h]	164,[e] 206,[e] 472,[e] 293[e,h]	
	E (LO) (cm^{-1})	176, 440, 688, 296[h]	175,[e] 443,[e] 687,[e] 293[e,h]	
	A_2 (cm^{-1})	274	278[e]	

[a]Reference 4.
[b]Reference 1(b).
[c]Reference 21(a).
[d]Reference 22(a).
[e]Reference 26(b).
[f]Reference 21(c).
[g]Reference 21(b).
[h]The nonpolar E-symmetry phonon frequency in $BaTiO_3$.

The incoherent approximation[33,34] is valid when the ratio of the volume of the reciprocal space covered in the experiment to the volume of the Brillouin zone is large. In our inelastic neutron scattering experiment, this ratio was about a few thousands. The data were properly averaged over the range of scattering angles to obtain the neutron-weighted generalized phonon density of states $g^n(E)$. The first-principles calculations were used to derive the generalized phonon density of states $g^n(E)$ for comparison with the experiments. The computed density of states was smeared with Gaussians with full width at half maximum of 1 meV for comparison with the experiments due to the finite resolution involved in the measurements.

III. RESULTS

A. Phonon dispersion relations and long-wavelength phonon frequencies

The calculated phonon dispersion relations of $PbTiO_3$ (Fig. 1) reveal giant anisotropies and span distinct spectral ranges for wave vector directions along (Γ-Z-A-R-Z) and perpendicular (Γ-M-X-Γ) to the direction of spontaneous polarization. Very limited single crystal inelastic neutron data[20] and first-principles calculations[4] of the phonon frequencies of $PbTiO_3$ were earlier reported and are in good agreement with our studies (Table I). The calculated transverse acoustic and transverse optic modes of $PbTiO_3$ (Fig. 1) propagating in

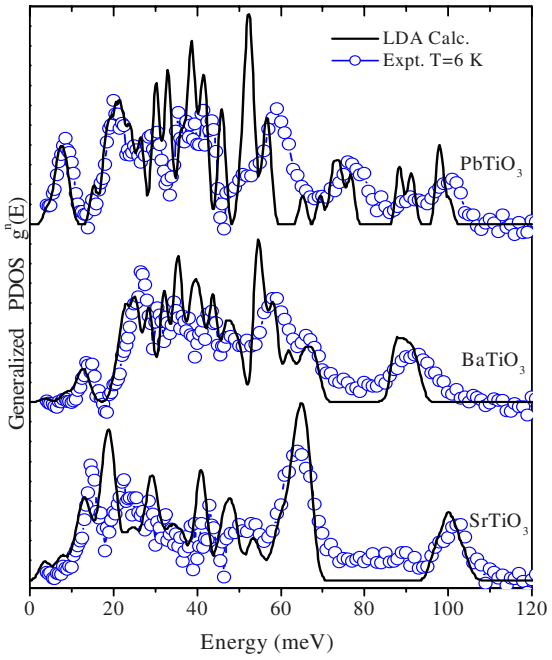

FIG. 2. (Color online) Comparison of the computed generalized phonon density of states with the measured inelastic neutron spectra ($T=6$ K) of tetragonal $PbTiO_3$, rhombohedral $BaTiO_3$, and the quantum paraelectric $SrTiO_3$.

the direction perpendicular to the spontaneous polarization show considerable splitting due to tetragonal anisotropy, which is in agreement with reported inelastic neutron data.[20(b)] LDA calculations of $PbTiO_3$ underestimate the strain (calculated $c/a=1.047$, observed $c/a=1.063$) and volume (calculated $V=60.4$ Å^3). As the phonon frequencies are quite sensitive to the structural parameters, we have relaxed the structural variables of $PbTiO_3$ at the observed lattice constants, as in earlier studies.[4] The computed structural parameters and long-wavelength phonon frequencies of tetragonal $PbTiO_3$ and rhombohedral $BaTiO_3$ are found to be in good agreement with reported experimental data[17(c),22(a)] and LDA calculations[4,26(b)] (Table I). The phonon dispersion relations of rhombohedral $BaTiO_3$ are plotted along cubic high symmetry directions (Fig. 1) to enable direct comparisons with the $\omega_j(\mathbf{q})$ of tetragonal $PbTiO_3$.

Symmetry analysis of the zone-center Γ-point phonon modes for the $P4mm$ space group of $PbTiO_3$ yields the classification Γ: $4A_1+5E+B_1$. The E-symmetry phonon modes are doubly degenerate. The A_1 and E phonon modes, which are both Raman and infrared active, are polar modes with vibrations which are, respectively, parallel and perpendicular to the direction of spontaneous polarization. For rhombohedral $BaTiO_3$, the phonon modes can be classified as Γ: $4A_1+5E+A_2$. The A_1 and four E modes are polar while the A_2 mode and a doubly degenerate E mode are nonpolar (Table I). While most of the calculated frequencies of $PbTiO_3$ are in good agreement with experiments (Table I), the observed E-symmetry polar infrared-active phonon modes[22(a)] at 289 (TO), 505 (TO), and 723 (LO) cm^{-1} at the Γ point are underestimated, which causes the shifting of the corresponding branches or peaks in the computed phonon dispersion relations and phonon density of states of $PbTiO_3$ (Figs. 1 and 2). Nevertheless, LDA calculations of $PbTiO_3$ bring out all the salient features and the calculated phonon dispersion relations and density of states are in good agreement overall with experiments.

Although experimentally $SrTiO_3$ is not ferroelectric even at low temperatures, it is very close to the ferroelectric threshold. Isotopic replacement of oxygen or partial cation substitution reduces quantum fluctuations and makes it ferroelectric.[14] Path-integral Monte Carlo simulations which include zero-point energy contributions yield the correct ground state[8] for ST. Neglect of zero-point energy in the structural relaxation yields ferroelectric zone-center instabilities for the polar E_u and A_{2u} phonon modes in the tetragonal $I4/mcm$ antiferrodistortive structure, which is in agreement with earlier reports.[5] LDA calculations of cubic $SrTiO_3$ yields soft zone-center and zone boundary R and M point phonon instabilities which is in good agreement with reported all electron linear augmented plane-wave calculations.[6] LDA calculations on a coarse wave vector mesh of the antiferrodistortive phase suggest that the phonon density of states of the tetragonal antiferrodistortive and cubic phases are quite similar overall.

Stirling[20(g)] and Cowley[20(i)] reported single crystal inelastic neutron scattering measurements at $T=90$ K and $T=296$ K of the low energy crystal dynamics and phonon dispersion relations in $SrTiO_3$. They fitted the observed inelastic neutron data to several lattice dynamics models with temperature dependent force constants.[20(g),20(i)] $SrTiO_3$ exhibits dynamical critical phenomena in the vicinity of the low temperature phase transition and the temperature variations of the soft-mode phonon frequencies and line shapes have aroused considerable interest.[20(j)] Our computed *ab initio* $T=0$ K phonon dispersion relations of cubic $SrTiO_3$ are compared to the reported $T=90$ K inelastic neutron scattering data[20(g),20(i)] [Fig. 1(c)]. Our calculations of cubic $SrTiO_3$ reveal very strong dispersion of the lowest energy optic phonon modes along the $(\xi\xi\xi)$ and $(\xi\xi 0)$ wave vector directions, which is in good agreement with reported inelastic neutron experiments[20(g),20(i)] [Fig. 1(c)]. While the higher frequency optic modes are in satisfactory agreement, the observed zone-center, R and M point soft modes in $SrTiO_3$ (which are found to be strongly temperature dependent[20(g),20(i)]) are in qualitative agreement with our $T=0$ K calculations. The computed phonon density of states of cubic and tetragonal $SrTiO_3$ neglecting effects from phonon instabilities are found to be in good agreement with our measured inelastic neutron scattering $T=6$ K data (Fig. 2).

B. Calculated charge densities and bonding characteristic of $PbTiO_3$, $BaTiO_3$, and $SrTiO_3$

The computed charge densities and isosurface plots of tetragonal $PbTiO_3$ and rhombohedral $BaTiO_3$ are given in Fig. 3. All densities were computed from the fully relaxed zero pressure LDA structures. The well connected region of charge between the Pb and O atoms indicate the strong covalent Pb-O bonding in PT. In $BaTiO_3$, the charge densities almost connect, while in cubic $SrTiO_3$, they are far from

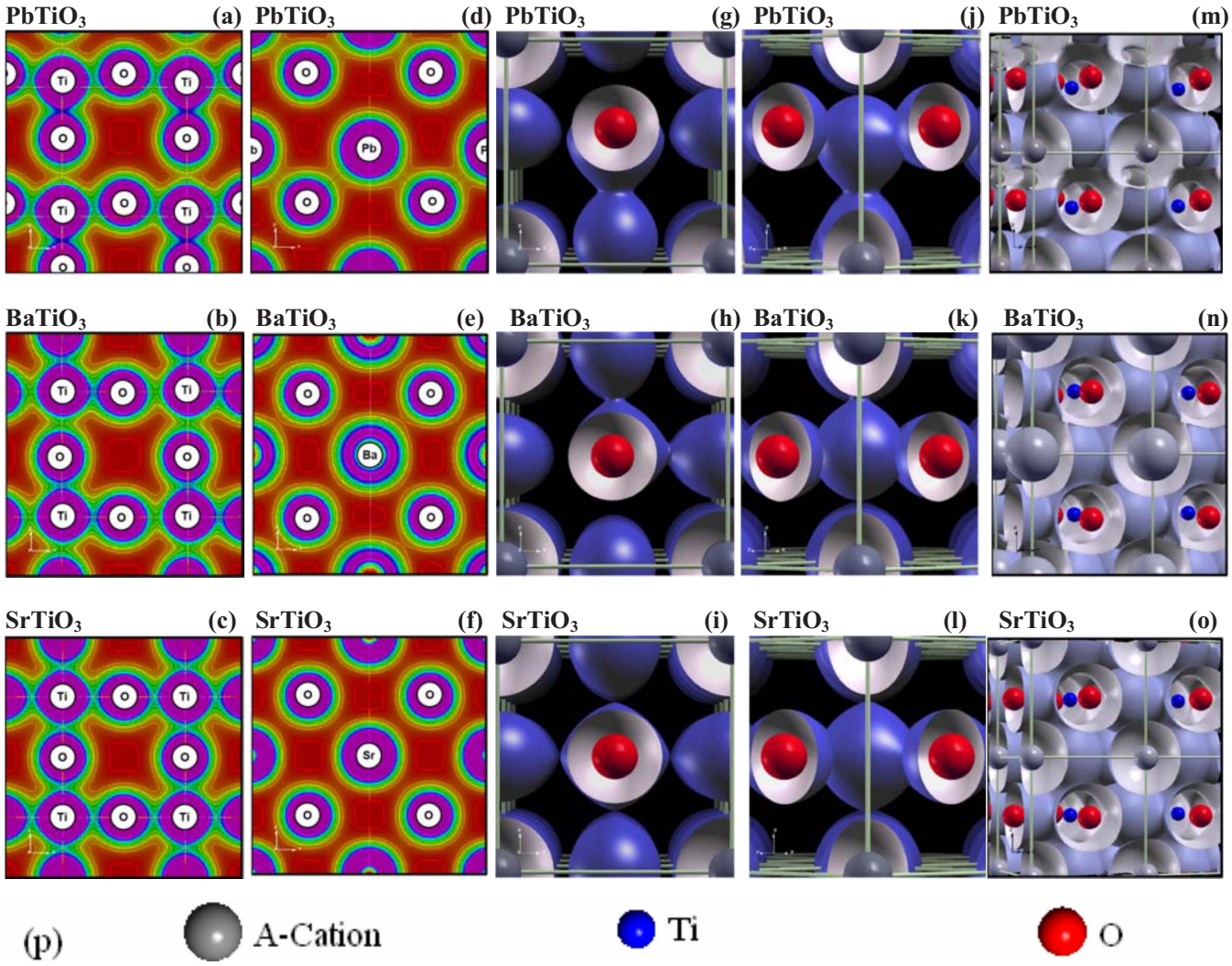

FIG. 3. (Color online) The computed [(a)–(f)] charge densities and [(g)–(o)] isosurface plots of tetragonal PT, rhombohedral BT, and cubic ST displayed using the code XCRYSDEN (Ref. 37). All densities were computed from the fully relaxed zero pressure LDA structures. The charge densities in [(a)–(c)] the [010] Ti-O plane and [(d)–(f)] the [010] Pb-O plane are shown. The 0.12 a.u. isosurfaces viewed down [100] and [110] are shown in (g)–(i) and (j)–(l), respectively, while the 0.03 a.u. isosurfaces are shown in (m)–(o). (p) The symbols used in (g)–(o) above.

connecting, which reveal ionic Ba-O and Sr-O bondings, respectively. Electronic structure calculations[3] reveal that the covalent bonding between the Ti and O in $PbTiO_3$ and $BaTiO_3$ arise from the hybridization between the titanium 3*d* states and the oxygen 2*p* states. This covalent Ti-O bonding was found to be essential for ferroelectricity in perovskites.[3] The strong covalency of the Pb-O bonds in tetragonal $PbTiO_3$, which arises from the hybridization of the Pb 6*s* state and O 2*p* state, has been theoretically predicted[3] as a key factor of the much larger ferroelectricity of $PbTiO_3$ as compared to that of $BaTiO_3$. The covalent character of the Pb-O bonds have been experimentally verified[16] and the computed charge densities are in good agreement with the observed density distributions of tetragonal $PbTiO_3$ and $BaTiO_3$ obtained from maximum entropy analysis of synchrotron data. The covalent nature of the Pb-O bond stabilizes the ferroelectric tetragonal phase in $PbTiO_3$, while the ionic nature of the Ba-O bond stabilizes the rhombohedral phase of $BaTiO_3$. These structural and bonding changes in these materials lead to important differences in their PDR (Fig. 1), PDOS (Fig. 2), as well as elastic, piezoelectric, and dielectric properties (Table II).

C. Elastic, piezoelectric, and dielectric properties

The computed elastic, piezoelectric, and dielectric properties of $PbTiO_3$ at the experimental volume (Table II) are in good agreement with reported room temperature Brillouin scattering data.[35] These demonstrate the intrinsic ability of DFPT calculations in accurately accounting for acoustic phonons and polarization. Electronic structure calculations[3] reveal that the hybridization between the titanium 3*d* states and the oxygen 2*p* states is essential for ferroelectricity in perovskites. The strong covalent character of the Pb-O bond (Fig. 3) in $PbTiO_3$ enhances its ferroelectric strength[3] as compared to $BaTiO_3$, wherein the Ba-O bonding is ionic. These bonding changes[3] between $PbTiO_3$ and $BaTiO_3$ give rise to significant differences in their Curie temperature,

TABLE II. Calculated spontaneous polarization P (C/m^2), elastic constants c_{ij} (GPa), and piezoelectric tensors e_{ij} (C/m^2) of tetragonal $PbTiO_3$ (PT) and rhombohedral $BaTiO_3$ (BT) compared to reported Brillouin (Refs. 35 and 36) and synchrotron x-ray diffraction [Ref. 21(a)] data. ε^∞ and ε^0 represent the electronic and zero frequency dielectric tensors (in units of ε_o), respectively. For $BaTiO_3$, the tensors are in their hexagonal coordinate system, with the z axis along the cubic (111) direction. The spontaneous polarization for $PbTiO_3$ and $BaTiO_3$ are, respectively, along the cubic [001] and [111] directions.

		P	c_{11}	c_{33}	c_{44}	c_{66}	c_{12}	c_{13}	c_{14}	c_{65}	e_{21}	e_{31}	e_{33}	e_{15}	e_{16}	ε^∞_{xx}	ε^∞_{zz}	ε^0_{xx}	ε^0_{zz}
PT	Expt. (Ref. 35)	0.75[a]	237	60	69	104	90	70				2.1	5.0	4.4				102	34
	Calc. (This work)	0.78	235	45	47	99	95	69	0	0	0	2.1	4.4	6.6	0	7.6	6.9	143	26
	Calc. (Ref. 11)		230	47	47	99	96	65				2.1	4.4	6.6					
BT	Calc. (This work)	0.28	251	236	37	89	73	36	45	45	2.3	2.3	3.7	4.6	2.3	6.1	5.5	51	27
	Calc. [Ref. 26(b)]		277	264	48	99	79	41	45	45	2.9	3.0	4.4	5.5	2.9	6.2	5.8	69	37

[a]Reference 21(e).

phase diagram, and electromechanical response (Table II). The large difference between the elastic constants C_{33} and C_{11} (Table II) in tetragonal $PbTiO_3$ reflects its inherent large anisotropy. This anisotropy is due to the large difference in the longitudinal acoustic phonon wave velocities for propagation along and perpendicular to the direction of polarization (Fig. 1). This anisotropy in $PbTiO_3$ leads to interesting directional enhancements of its piezoresponse (Table II). The enhanced values for e_{33} and e_{15} in tetragonal $PbTiO_3$ are due to the large atomic response to the corresponding macroscopic strains combined with large anomalous values of the Born effective charge tensors.

The computed partial density of states giving the dynamical contributions from various atoms are given in Fig. 4. These reveal that the 0–20 meV low frequency vibrations which critically govern the electromechanical response are strongly influenced by the A-O bonding character. The strong covalent bonding of the Pb-O bonds (Fig. 3) contributes to the strong anisotropy of the elastic and piezoelectric response of $PbTiO_3$ (Table II). Although first-principles calculations of the piezoelectric response in $PbTiO_3$ and $BaTiO_3$ have also been reported by others,[11,26] in this work, we have examined the intimate connections between phonon spectra and electromechanical response. The computed elastic, piezoelectric, and dielectric constants (Tables I and II) are found to be quite sensitive to the relaxed structural parameters and although our results for $PbTiO_3$ are similar to earlier first-principles results,[11] our results for $BaTiO_3$ have some differences with reported values,[26(b)] which are due to the differences in their computed crystal structures.

D. Phonon density of states and partial density of states

The computed generalized phonon density of states is in good agreement with the observed inelastic neutron scattering spectra (Fig. 2) and spans the spectral range from 0 to 120 meV. The phonon spectrum of the quantum paraelectric $SrTiO_3$ is found to be fundamentally distinct

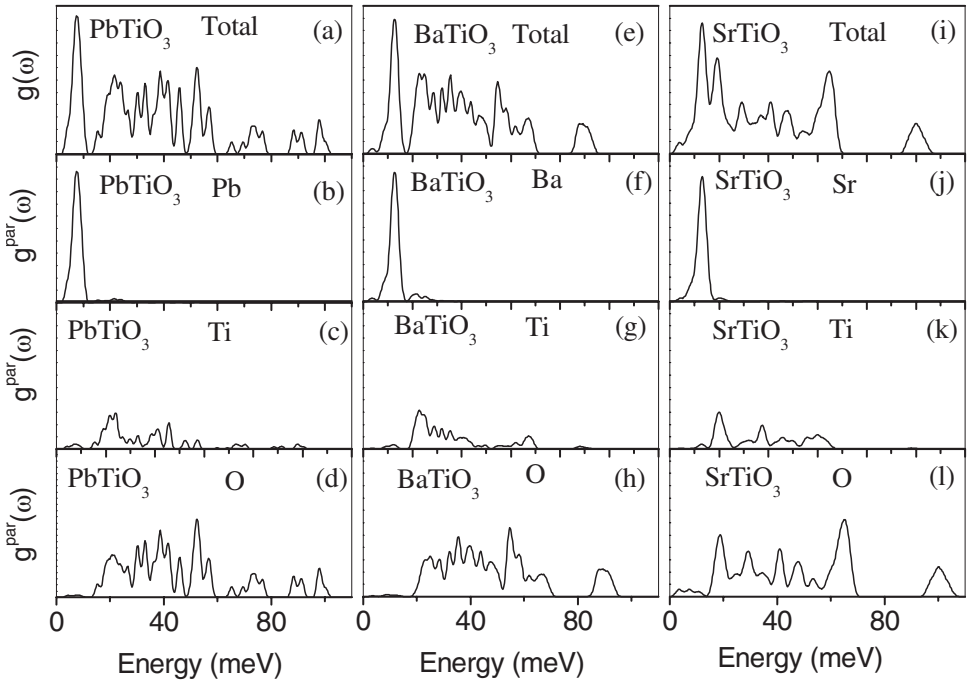

FIG. 4. The computed total and partial densities of states of tetragonal $PbTiO_3$, rhombohedral $BaTiO_3$, and cubic $SrTiO_3$ (energy $E=\hbar\omega$). For cubic $SrTiO_3$, effects from phonon instabilities are neglected.

from those of ferroelectric $PbTiO_3$ and $BaTiO_3$, with a large, 70–90 meV, phonon band gap. This large phonon band gap is due to the distinct bonding in $SrTiO_3$ (Fig. 3) as compared to ferroelectric $PbTiO_3$ and $BaTiO_3$. From the viewpoint of crystal stability,[9,14] the quantum paraelectricity in the threshold of ferroelectric behavior in $SrTiO_3$ originates from the critical status of this material. Such trends are conventionally studied[9,14] using the tolerance factor $[t=(r_{Sr}+r_O)/\sqrt{2}(r_{Ti}+r_O)]$. By using reported ionic radii, the tolerance was found to be $t=1.00$ for $SrTiO_3$, which means that the ion packing in $SrTiO_3$ is ideal for a perovskite-type structure.[14] The tolerance t for $BaTiO_3$ and $PbTiO_3$ are similarly[9] 1.07 and 1.03. Larger ($t>1$) and smaller ($t<1$) values were found to favor ferroelectricity (e.g., $BaTiO_3$) and quantum paraelectricity (e.g., see Ref. 9: $CaTiO_3$, $t=0.97$), respectively. The critical status of $SrTiO_3$ and its distinct bonding as compared to $PbTiO_3$ and $BaTiO_3$ result in spectacular signatures in the phonon spectra.

The computed partial density of states (Fig. 4) enables microscopic interpretations of the observed data. These reveal that while the *A* cations (namely, the Pb, Ba, and Sr) contribute in the 0–20 meV spectral range (Fig. 4), the intermediate and high energy spectra are due to the Ti and O vibrations. The phonon spectra (neglecting instabilities) are overall similar in the paraelectric cubic and tetragonal antiferrodistortive phases of $SrTiO_3$ because the distortions for the SrO_{12} and TiO_6 polyhedra are small in the antiferrodistortive tetragonal phase of $SrTiO_3$. On the other hand, the covalent Ti-O bonding, which is found to be essential for ferroelectricity in perovskites, causes a strong distortion of the Ti-O_6 octahedra and the spectra are significantly different in the ferroelectric and paraelectric phases of $PbTiO_3$ and $BaTiO_3$. For example, in tetragonal $PbTiO_3$, the calculated Ti-O bond lengths (Å) are 1.9785(4), 1.7606(1), and 2.3908(1) (where the values in parentheses give the multiplicity of the bonds), which significantly deviate from the typical Ti-O bond length of about 1.95 Å in cubic perovskites. This strong TiO_6 octahedral distortion (Table I) characteristic of ferroelectric behavior is responsible for the filling up of the characteristic 70–90 meV phonon band gap of the quantum paraelectric $SrTiO_3$. Strong covalency of the Pb-O bonds similarly distorts the PbO_8 polyhedra [2.8016(4) Å; 2.5243(4) Å] in tetragonal $PbTiO_3$, which leads to the following: (i) The vibrations of the Pb atoms in $PbTiO_3$ (around 7.5 meV) are considerably softer than in the vibrations of Ba (around 12.5 meV) in $BaTiO_3$ and Sr (around 13 meV) in $SrTiO_3$ and (ii) there are significant differences in the elastic and piezoelectric properties of $PbTiO_3$ and $BaTiO_3$ (Table II).

IV. DISCUSSION

A large, 70–90 meV, phonon band gap seems characteristic of $ATiO_3$ perovskite quantum paraelectrics such as $SrTiO_3$. In the case of the ferroelectric instability, the covalent interactions, which play a predominant role,[3] lead to marked differences in the phonon spectra. Ferroelectricity in perovskites arises from competition between the Coulomb (which favors ferroelectric) and short-ranged (which favors paraelectric) interactions.[3] This competition, which contributes to several reported anomalies,[2–23] also leads to the spectacular signatures in the phonon spectra. The covalent Ti-O bonding (Fig. 3) found necessary for ferroelectric behavior in perovskites[3] causes the following: (i) the large 70–90 meV phonon band gap of paraelectric $SrTiO_3$ gets filled by the covalent Ti-O vibrations in ferroelectric $PbTiO_3$ and $BaTiO_3$ and (ii) there are giant anisotropies in the phonon spectra and electromechanical response of $PbTiO_3$ (due to the combined Ti-O and Pb-O covalent bondings). The anisotropy of the phonon spectra correlates well with the ferroelectric and piezoelectric strengths. These results suggest that vibrational spectroscopy can aid in the search for novel materials. The distinct phonon spectra of $PbTiO_3$, $BaTiO_3$, and $SrTiO_3$ lead to important differences in their thermodynamic properties and phase diagram.

Similar studies as reported in this work are highly desirable for multiferroics, which simultaneously exhibit ferroelectricity and magnetism. Ferroelectricity in perovskites often occurs due to ligand-field hybridization of the B cation by its surrounding oxygen,[3] which gives rise to the off-centered displacement in common perovskite ferroelectrics such as $BaTiO_3$ and $Pb(Zr,Ti)O_3$. Since such a mechanism requires that the *d* orbitals on the small B cation are formally unoccupied, it precludes the coexistence of ferroelectricity and ferromagnetism, which requires occupied *d* orbitals.[38] Another mechanism for ferroelectricity occurs around cations that have an $(ns)^2$ valence electron configuration which tends to lose inversion symmetry invoking a mixing between the $(ns)^2$ ground state and a low-lying $(ns)^1(np)^1$ excited state. This occurs only if the ionic site does not have inversion symmetry and this "stereochemical activity of the lone pair" is the driving force for off-centered distortion in Bi-based perovskites, such as $BiMnO_3$ and $BiFeO_3$.[38] In this mechanism, both ferroelectricity and magnetism can coexist and several known multiferroics such as $BiFeO_3$ belong to this latter class of ferroelectrics. In $BaTiO_3$, only the first mechanism is prevalent,[38] while both these mechanisms occur in $PbTiO_3$, since the Pb off-centered displacements arise from such "stereochemical activity of the lone pair." These differences between $PbTiO_3$ and $BaTiO_3$ give rise to important differences in their ferroelectric, piezoelectric, and dielectric behaviors (Table II) as well as contribute to spectacular changes in their phonon spectra (Figs. 1 and 2).

Manipulation of the crystal structure or chemistry[38] provides an alternative and elegant mechanism for ferroelectricity which permits it to occur in spite of the simultaneous occurrence of magnetic ordering. Yet another mechanism of ferroelectricity occurs in multiferroic $YMnO_3$ which arises from a buckling of the MnO_5.[38] In striking contrast to the mechanisms described above, there is no rehybridization or change in chemical bonding between the paraelectric and ferroelectric phases.[38] Such a mechanism offers a different route for designing magnetic ferroelectrics which are very appealing for spintronics applications. It will be interesting to understand how these various mechanisms of ferroelectricity influence their phonon properties.

An important objective of this study was the integration of current advances in first-principles computational theory with neutron experiments to provide microscopic insights

that can define new strategies for the screening of novel materials. To transform the theoretical quantum mechanical techniques[24–27] developed in the past several decades into predictive design and discovery tools, important tests of the ability of modern first-principles theory in reproducing various macroscopic physical properties of ferroelectrics were of interest. In this context, we have compared our calculations to reported[15–23] Raman and infrared data (Table I), inelastic neutron data[20] (Figs. 1 and 2), Brillouin data[35] (Table II), and synchrotron x-ray data[16] of three classic perovskites in addition to comparing with our experimental neutron data. Our calculations are in good agreement with these experimental studies. The theoretical studies predict giant anisotropies in the phonon dispersion relations and electromechanical response of $PbTiO_3$, which arise due to the strongly "directional" character of the covalent interactions found necessary for ferroelectricity. This anisotropy in the phonon dispersion relations obtained from first-principles calculations of $PbTiO_3$ (particularly for the high energy modes which have not been studied earlier[20]) is measurable experimentally via future single crystal inelastic neutron scattering and inelastic x-ray scattering measurements. Anisotropy in the phonon spectra of $PbTiO_3$ obtained from LO-TO splittings have been measured using single-crystal infrared spectroscopic studies and are found to be in good agreement with our calculations (Table I).

V. CONCLUSIONS

In summary, we report very successful tests of the ability of first-principles theory in reproducing the experimental data of phonon dispersion relations, density of states, and electromechanical response of three classic perovskites, $PbTiO_3$, $BaTiO_3$, and $SrTiO_3$. We obtain an important correlation between the phonon spectra and ferroelectricity in perovskites, which can guide future efforts at custom designing still more effective piezoelectrics for applications. A large phonon band gap seems characteristic of $ATiO_3$ perovskite quantum paraelectrics, while anisotropy of the phonon spectra correlates well with the ferroelectric strength. Distinct bonding characteristics in the ferroelectric and paraelectric phases give rise to these vibrational signatures. Although we have studied only three classic perovskites, since the vibrational signatures we obtain arise due to the fundamental differences in the physics of ferroelectric (covalently bonded) and paraelectric systems, we believe that these correlations in phonon spectra could be universal. Our results suggest that vibrational spectroscopy can aid in the search for novel materials. We hope these studies will stimulate interest in systematic investigations of other ferroelectrics to examine the universalities of our observations. Such studies are particularly desirable for multiferroics such as $YMnO_3$, which simultaneously exhibit ferroelectricity and magnetic properties, and which involve very different mechanisms of ferroelectricity[38] from those observed in classic perovskites such as $PbTiO_3$ and $BaTiO_3$. The excellent agreement between theory and experiments demonstrates the intrinsic power of first-principles quantum mechanical calculations for deriving various key properties of these materials.

ACKNOWLEDGMENTS

N.C. thanks R. E. Cohen and S. L. Chaplot for discussions. This research used the supercomputing resources at the Bhabha Atomic Research Centre (BARC) and the Center for Piezoelectrics by Design, College of William and Mary (E.J.W.). The work at Argonne National Laboratory was supported by the Office of Basic Energy Sciences, Division of Materials Sciences, U.S. Department of Energy, under Contract No. W-31-109-ENG-38.

[1] M. E. Lines and A. M. Glass, *Principles and Applications of Ferroelectrics and Related Materials* (Clarendon, Oxford, 1977); F. Jona and G. Shirane, *Ferroelectric Crystals* (Dover, New York, 1993).
[2] P. Ghosez, E. Cockayne, U. V. Waghmare, and K. M. Rabe, Phys. Rev. B **60**, 836 (1999).
[3] R. E. Cohen, Nature (London) **358**, 136 (1992).
[4] A. García and D. Vanderbilt, Phys. Rev. B **54**, 3817 (1996).
[5] N. Sai and D. Vanderbilt, Phys. Rev. B **62**, 13942 (2000).
[6] C. Lasota, C.-Z. Wang, R. Yu, and H. Krakauer, Ferroelectrics **194**, 109 (1997).
[7] W. Zhong, R. D. King-Smith, and D. Vanderbilt, Phys. Rev. Lett. **72**, 3618 (1994).
[8] W. Zhong and D. Vanderbilt, Phys. Rev. B **53**, 5047 (1996).
[9] W. Zhong and D. Vanderbilt, Phys. Rev. Lett. **74**, 2587 (1995).
[10] H. Fu and R. E. Cohen, Nature (London) **403**, 281 (2000).
[11] Z. Wu and R. E. Cohen, Phys. Rev. Lett. **95**, 037601 (2005); G. Sághi-Szabó, R. E. Cohen, and H. Krakauer, *ibid.* **80**, 4321 (1998).
[12] I. A. Kornev, L. Bellaiche, P. Bouvier, P.-E. Janolin, B. Dkhil, and J. Kreisel, Phys. Rev. Lett. **95**, 196804 (2005); I. I. Naumov and H. Fu, Phys. Rev. B **72**, 012304 (2005); H. Fu and L. Bellaiche, Phys. Rev. Lett. **91**, 057601 (2003); B. P. Burton and E. Cockayne, Phys. Rev. B **60**, R12542 (1999); M. Ghita, M. Fornari, D. J. Singh, and S. V. Halilov, Phys. Rev. B **72**, 054114 (2005).
[13] M. Ahart, M. Somayazulu, R. E. Cohen, P. Ganesh, P. Dera, H. K. Mao, R. J. Hemley, Y. Ren, P. Liermann, and Z. Wu, Nature (London) **451**, 543 (2008).
[14] M. Itoh, R. Wang, Y. Inaguma, T. Yamaguchi, Y.-J. Shan, and T. Nakamura, Phys. Rev. Lett. **82**, 3540 (1999).
[15] K. A. Müller and H. Burkard, Phys. Rev. B **19**, 3593 (1979).
[16] Y. Kuroiwa, S. Aoyagi, A. Sawada, J. Harada, E. Nishibori, M. Takata, and M. Sakata, Phys. Rev. Lett. **87**, 217601 (2001).
[17] (a) B. Zalar, V. V. Laguta, and R. Blinc, Phys. Rev. Lett. **90**, 037601 (2003); (b) E. A. Stern, *ibid.* **93**, 037601 (2004); (c) M. Dawber, C. Lichtensteiger, M. Cantoni, M. Veithen, P. Ghosez, K. Johnston, K. M. Rabe, and J.-M. Triscone, *ibid.* **95**, 177601 (2005).
[18] A. A. Sirenko, I. A. Akimov, J. R. Fox, A. M. Clark, H. C. Li, W. Si, and X. X. Xi, Phys. Rev. Lett. **82**, 4500 (1999).
[19] D. E. Grupp and A. M. Goldman, Phys. Rev. Lett. **78**, 3511

(1997).

[20] (a) I. Tomeno, Y. Ishii, Y. Tsunoda, and K. Oka, Phys. Rev. B **73**, 064116 (2006); (b) J. Hlinka, M. Kempa, J. Kulda, P. Bourges, A. Kania, and J. Petzelt, *ibid.* **73**, 140101(R) (2006); (c) G. Shirane, Rev. Mod. Phys. **46**, 437 (1974); (d) G. Shirane, B. C. Frazer, V. J. Minkiewicz, and J. A. Leake, Phys. Rev. Lett. **19**, 234 (1967); (e) G. Shirane, J. D. Axe, J. Harada, and J. P. Remeika, Phys. Rev. B **2**, 155 (1970); (f) G. Shirane, J. D. Axe, J. Harada, and A. Linz, *ibid.* **2**, 3651 (1970); (g) W. G. Stirling, J. Phys. C **5**, 2711 (1972); (h) B. Jannot, C. Escribe-Filippini, and J. Bouillot, *ibid.* **17**, 1329 (1984): (i) R. A. Cowley, Phys. Rev. **134**, A981 (1964); (j) D. A. Bruce and W. G. Stirling, J. Phys. C **16**, 841 (1983).

[21] (a) R. J. Nelmes and W. F. Kuhs, Solid State Commun. **54**, 721 (1985); (b) G. H. Kwei, A. C. Lawson, S. J. L. Billinge, and S.-W. Cheong, J. Phys. Chem. **97**, 2368 (1993); (c) A. W. Hewat, Ferroelectrics **6**, 215 (1974); (d) A. Sani, M. Hanfland, and D. Levy, J. Phys.: Condens. Matter **14**, 10601 (2002); (e) V. G. Gavrilyachenko, R. I. Spinko, M. A. Martynenko, and E. G. Fesenko, Sov. Phys. Solid State **12**, 1203 (1970).

[22] (a) J. D. Freire and R. S. Katiyar, Phys. Rev. B **37**, 2074 (1988); (b) C. M. Foster, M. Grimsditch, Z. Li, and V. G. Karpov, Phys. Rev. Lett. **71**, 1258 (1993); (c) J. Petzelt, T. Ostapchuk, I. Gregora, I. Rychetský, S. Hoffmann-Eifert, A. V. Pronin, Y. Yuzyuk, B. P. Gorshunov, S. Kamba, V. Bovtun, J. Pokorný, M. Savinov, V. Porokhonskyy, D. Rafaja, P. Vaněk, A. Almeida, M. R. Chaves, A. A. Volkov, M. Dressel, and R. Waser, Phys. Rev. B **64**, 184111 (2001).

[23] B. D. Chapman, E. A. Stern, S.-W. Han, J. O. Cross, G. T. Seidler, V. Gavrilyatchenko, R. V. Vedrinskii, and V. L. Kraizman, Phys. Rev. B **71**, 020102(R) (2005).

[24] For a review on DFPT, see S. Baroni, S. de Gironcoli, A. D. Corsco, and P. Giannozzi, Rev. Mod. Phys. **73**, 515 (2001).

[25] X. Gonze, Phys. Rev. B **55**, 10337 (1997); X. Gonze and C. Lee, *ibid.* **55**, 10355 (1997).

[26] (a) D. R. Hamann, X. Wu, K. M. Rabe, and D. Vanderbilt, Phys. Rev. B **71**, 035117 (2005); (b) X. Wu, D. Vanderbilt, and D. R. Hamann, *ibid.* **72**, 035105 (2005); (c) M. Veithen, X. Gonze, and P. Ghosez, *ibid.* **71**, 125107 (2005).

[27] R. Resta, Rev. Mod. Phys. **66**, 899 (1994); R. D. King-Smith and D. Vanderbilt, Phys. Rev. B **47**, 1651 (1993).

[28] X. Gonze, J.-M. Beuken, R. Caracas, F. Detraux, M. Fuchs, G.-M. Rignanese, L. Sindic, M. Verstraete, G. Zerah, F. Jollet, M. Torrent, A. Roy, M. Mikami, Ph. Ghosez, J.-Y. Raty, and D. C. Allan, Comput. Mater. Sci. **25**, 478 (2002); the ABINIT code is a collaborative project of the Universite Catholique de Louvain, Corning, Inc., and other collaborators (http://www.abinit.org/).

[29] http://www.sourceforge.net/

[30] A. M. Rappe, K. M. Rabe, E. Kaxiras, and J. D. Joannopoulos, Phys. Rev. B **41**, 1227 (1990).

[31] N. Choudhury, Z. Wu, E. J. Walter, and R. E. Cohen, Phys. Rev. B **71**, 125134 (2005); N. Choudhury, R. E. Cohen, and E. J. Walter, Comput. Mater. Sci. **37**, 152 (2006).

[32] N. Choudhury and S. L. Chaplot, Phys. Rev. B **73**, 094304 (2006).

[33] S. L. Chaplot, N. Choudhury, S. Ghose, M. N. Rao, R. Mittal, and P. Goel, Eur. J. Mineral. **14**, 291 (2002); B. Dorner, *Coherent Inelastic Neutron Scattering in Lattice Dynamics* (Springer-Verlag, Berlin, 1982); C.-K. Loong, P. Vashishta, R. K. Kalia, M. H. Degani, D. L. Price, J. D. Jorgensen, D. G. Hinks, B. Dabrowski, A. W. Mitchell, D. R. Richards, and Y. Zheng, Phys. Rev. Lett. **62**, 2628 (1989); N. Choudhury, S. Ghose, C. P. Chowdhury, C.-K. Loong, and S. L. Chaplot, Phys. Rev. B **58**, 756 (1998); K. R. Rao, S. L. Chaplot, N. Choudhury, S. Ghose, and D. L. Price, Science **236**, 64 (1987).

[34] J. M. Carpenter and D. L. Price, Phys. Rev. Lett. **54**, 441 (1985); D. L. Price and K. Skold, in *Neutron Scattering*, edited by K. Skold and D. L. Price (Academic, Orlando, 1986).

[35] A. G. Kalinichev, J. D. Bass, B. N. Sun, and D. A. Payne, J. Mater. Res. **12**, 2623 (1997).

[36] The signs of the piezoelectric constants are related to the choice of the coordinate axis.

[37] A. Kokalj, Comput. Mater. Sci. **28**, 155 (2003).

[38] B. B. Van Aken, T. M. Palstra, A. Filippetti, and N. A. Spaldin, Nat. Mater. **3**, 164 (2004); N. A. Spaldin and W. E. Pickett, J. Solid State Chem. **176**, 615 (2003); N. A. Hil, Annu. Rev. Mater. Res. **32**, 1 (2002).